Modelling the Stiffness Development in Asphalt Concrete to Obtain Fatigue Failure Criteria

Anqi Chen[1, 2, *], Gordon D. Airey[1], Nick Thom[1], Jack Litherland[3], Rufus Adjetey Nii-Adjei [1]

1. Nottingham Transportation Engineering Centre, Faculty of Civil Engineering, University of Nottingham, University Park, Nottingham NG7 2RD, United Kingdom; E-mail address: gorden.airey@nottingham.ac.uk (GD. Airey); nick.thom@nottingham.ac.uk (N. Thom). rufus.adjetey@nottingham.ac.uk (R.N Adjetey)

2. School of Transportation, Southeast University, Nanjing, Jiangsu 210096, China

3. Resilience Engineering Research Group, Faculty of Civil Engineering, University of Nottingham, University Park, Nottingham NG7 2RD, United Kingdom; E-mail address: jitherland@hotmail.co.uk (J. Litherland).

* Correspondence author. E-mail address: anqi.chen@nottingham.ac.uk (A. Chen).

Abstract:

The study of fatigue is critical to good usability and durability of asphalt pavements. Inaccurate calculation of the fatigue failure criteria can cause incorrect evaluation of the fatigue performance, leading to inaccurate prediction of the pavement performance and poor maintenance planning. This paper develops a stiffness change tendency method (SCTM) that can be used to model the stiffness evolution in asphalt concrete and determine critical laboratory fatigue failure points to characterise different fatigue damage stages. A logistic model was selected to represent the relationship between the log of the stiffness (E) and the log of the number of cycles (N) obtained from two-point bending (2PB) fatigue tests. The measured stiffness reduction versus loading curves were determined for a range of asphalt mixtures in unaged, aged and moisture damaged conditions by testing at various temperatures and strains. By analysing the derivatives of the logistic model, it is possible to identify three transition points associated with fatigue progression. There is good agreement between the laboratory data and the logistic model proposed, confirming that the logistic model is a good approximation to the stiffness reduction curves. The number of loading cycles associated with the first two transition points in the SCTM (N_{P1} and N_{P2}) were compared to the value of N_1 and N_{fm} obtained from the energy ratio (ER) method and the ratio of dissipated energy change (RDEC) method, respectively. There are no statistically differences between the SCTM and two energy-based methods, proving that P1 can be viewed as the number of cycles to micro-crack initiation and propagation, and P2 can be defined as the macro-crack generation point (the true failure point). Three different mixtures are subjected to four-point bending (4PB) fatigue tests to demonstrate the applicability of the SCTM with different bitumen types, mixture grades and test methods. The SCTM provides a method to model stiffness development, obtain different fatigue failure criteria and characterise different fatigue damage stages, which could be useful in a simulation of pavement deterioration.

Keywords: asphalt mixtures, fatigue, stiffness loss, dissipated energy, pavement performance

Highlights

- The 2PB test is used to develop a stiffness change tendency method (STCM).
- The stiffness development is modelled by the STCM.
- The value of the transition points is compared against traditional energy-based methods.
- The SCTM is applicable for different bitumen grades, mixture grades and test methods

1 Introduction

Asphalt pavements are the main type of pavement structure used in road networks worldwide. With increasing vehicle numbers and higher traffic loads, there is a continuous need to improve the performance of asphalt pavements to maintain serviceability. One of the main distresses experienced by asphalt pavements is fatigue damage resulting from gradual weakening of pavements as a function of cumulative traffic loading cycles. Considerable research has been undertaken to explore methods to reduce the effect of fatigue damage and prolong the pavement life, critical to this is the accurate identification of the key stages during the fatigue performance deterioration and the appropriate selection of failure criteria [1-5].

Within the literature, various approaches have been used to define fatigue damage and analyse fatigue performance. Traditionally, fatigue failure is defined using a phenomenological approach with the fatigue failure criterion being defined as the number of loading cycles corresponding to a 50% stiffness reduction [6]. The traditional fatigue failure criterion is easy for calculation and prediction of the fatigue life, but results in the loss of information regarding fatigue behaviour characteristics. It is realized that a typical fatigue curve (stiffness versus number of cycles under strain-controlled mode) is presented by a "S" shaped curve with four distinct regions (internal heating, micro-crack formation, crack formation and propagation, and sample breakdown) separated by three transition points [7-8]. It is then suggested that the first and second transition points are possibly associated with microcracking and macrocracking in the material, respectively [9]. But the method of how to determine the transition points on the stiffness reduction curve, and how to relate the transition points to different fatigue cracking processes are still not very clear.

A range of energy-based approaches have subsequently been proposed as improved methods to characterise fatigue damage. The cumulative dissipated energy (CDE) approach and initial dissipated energy (IDE) approach are two of the earliest examples of this [8,10]; however, only a proportion of the energy dissipation happening in asphalt materials during the loading-unloading process is due to fatigue damage. Further methodologies to isolate the energy dissipation due to damage and viscoelasticity, including the ratio of dissipated energy change (RDEC), dissipated pseudo-strain energy (DPSE) and rate of DPSE approaches, were subsequently developed [2,11-12]. Different from the traditional method, energy-based approaches are independent of test conditions and mode of loading when nonlinearity in material response is not significant [13-14]. More importantly, by calculating the plot of dissipated energy versus number of cycles, three stages that were clearly separated by two transition points were found. The transition points were then used as fatigue criteria that were defined and calculated using the energy-based approaches. Pronk and Hopman [15] used the energy ratio (ER) to define the number of cycles at a critical fatigue point (N_1) where the relationship between the ER and the number of cycles becomes nonlinear, for

controlled strain fatigue tests. Pronk [16] then suggested that N_1 could be defined as the number of cycles at which cracks are considered to initiate. Ghuzlan and Carpenter [11] used the RDEC to define macroscopic failure (N_{fm}), which is related to crack propagation. The RDEC method was refined by Shen and Carpenter to calculate the value of N_{fm} [17]. Although these energy-based approaches greatly improve the ability to determine the appropriate failure criteria by relating criteria to crack initiation and propagation, they have a limitation in that the defined failure criteria cannot be directly connected to the stiffness development (strain-stress change).

This paper combines the benefits of both approaches (phenomenological and energy-based) by developing a method that can be used to model the stiffness evolution in asphalt concrete, determine critical laboratory fatigue failure points to characterise different fatigue damage stages, and relate the fatigue failure points to different fatigue cracking processes. This aim is achieved by selecting a logistic model to represent the relationship between the log of the stiffness (E) and the log of the number of cycles (N) obtained from two-point bending (2PB) fatigue tests to form a stiffness change tendency method (SCTM). The measured stiffness reduction versus loading curves were determined for a range of asphalt mixtures in unaged, aged and moisture damaged conditions by testing at various temperatures and strains. By analysing the derivatives of the logistic model, it is possible to identify three transition points associated with fatigue progression. The number of loading cycles associated with the first two transition points in the SCTM (N_{p1} and N_{p2}) were compared to the value of N_1 and N_{fm} obtained from two energy-based approaches (the ER and RDEC approaches), aiming to relate N_{p1} and N_{p2} to crack initiation and propagation. Finally, three different mixtures are subjected to four-point bending (4PB) fatigue tests to demonstrate the applicability of the SCTM in more bitumen grades, mixture grades and test methods.

2 Materials and Experimental Methods

2.1 Raw Materials and Mixture Design

Three asphalt concretes, namely the dense aggregate gradation bituminous mixture with NMAs of 14 mm (DBM -14) with a 40/60 penetration grade bitumen (Pen40/60), the dense aggregate gradation bituminous mixture with NMAs of 10 mm (DBM-10) with a crumb rubber modified bitumen (CRMB) and stone mastic asphalt with NMAs of 10 mm (SMA-10) + Pen40/60 were used for the comparison of the fatigue failure criteria of different asphalt concretes with different NMAs or bitumen types. The physical properties of Pen40/60 and CRMB are shown in Table 1. The aggregate gradings [18] for these three asphalt concretes are shown in Figure 1. Asphalt mixtures were compacted by a roller compactor with mixing and compaction procedures of the asphalt mixtures chosen from BS EN 12697-35: 2016 [19] and BS EN 12697-33: 2019 [20]. Hot mixture is poured into a pre-heated square mould (305 ×305 mm^2) and compacted to the required slab thickness.

For the 2PB test, the DBM -14 + Pen40/60 mixture was used with granite aggregates and the bitumen content was 5% by the weight of the mixture. For the 4PB test, three different mixtures including DBM-14 + CRMB, DBM-10 + Pen 40/60 and SMA-10 + Pen 40/60 were tested. The hot mixture is poured into pre-heated moulds of dimensions 400 mm × 300 mm and compacted to the required slab thickness of 80 mm to obtain the desired air

void content (7%). The target bitumen content was 5.5% for the DBM and 6.1% for the SMA. Prismatic rectangular beams were cut out of these slabs with specified dimensions. Regarding the dimensions, the tolerance requirements of 380 ± 6 mm in length, 50 ± 2 mm in height, and 63 ± 2 mm in width as required by the AASHTO T321 and ASTM D7460-10 were met.

Table 1: Properties of bitumen.

Properties	Pen 40/60	CRMB	Test methods
Specific gravity	1.030	1.040	BS 2000-549:2007 [21]
Penetration (25℃, 5 s, 100 g)/0.1 mm	43	33	BS EN 1426:2015 [22]
Softening point/℃	51.1	59.6	BS EN 1427:2015 [23]
Viscosity, 135℃/Pa.s	0.441	1.78	BS EN 13302:2018 [24]

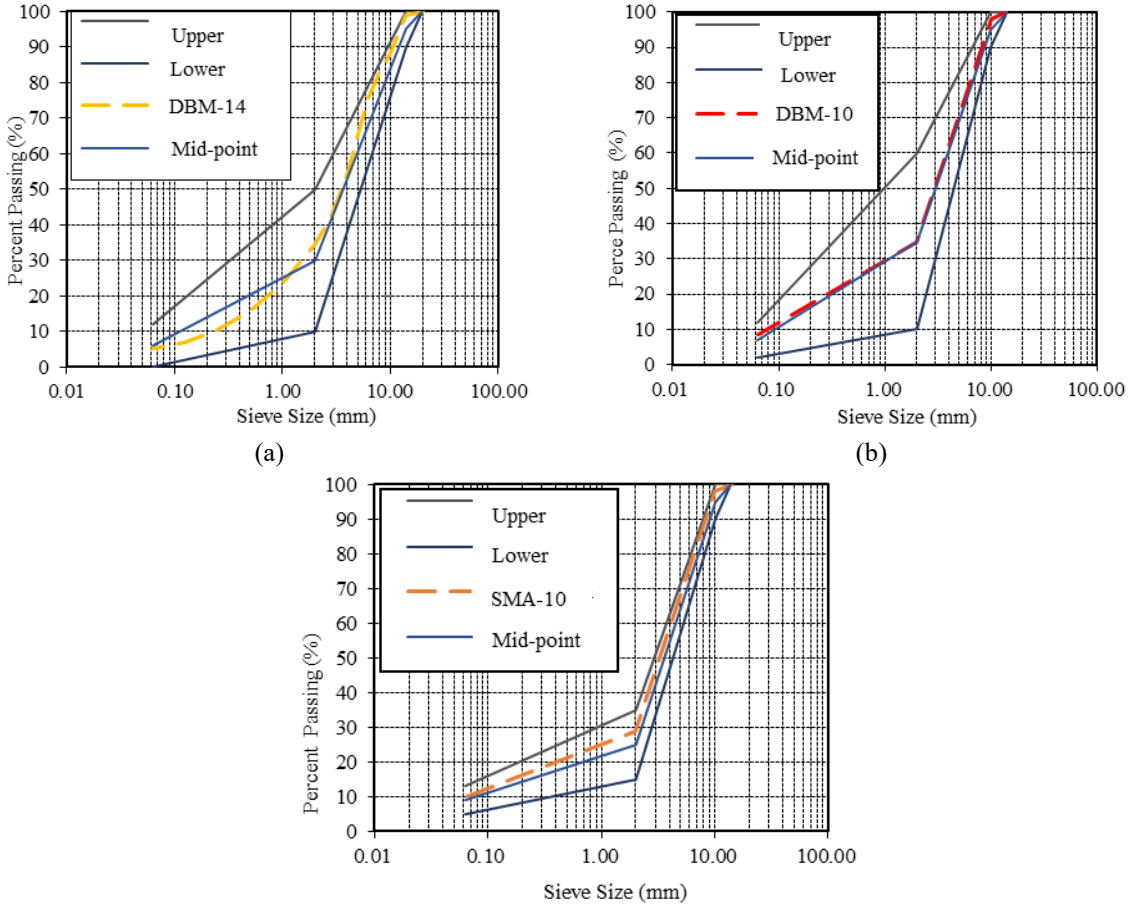

Figure 1: Gradations of (a) DBM-14, (b) DBM-10 and (c) SMA-10.

2.2 Specimen Fabrication and Test Methods

2.2.1 Thermal Oxidative Ageing Tests

The test method for short-term ageing of the asphalt mixture was to put loose material in an oven at 135 ± 1 ℃ for 4 hours. For long-term ageing, the compacted specimens were put in an oven at 85 ± 3 ℃ for 5 days according to TS 12697-52:2017 [25]. The oven setting is presented in Figure 2. After the ageing period, the oven is turned off and left to cool to room temperature and the specimens are then removed. All the specimens were placed in a temperature-controlled cabinet at 20 °C for at least 6 hours before testing. The materials after short-term and long-term ageing can be seen in Figures 2 (a) and (b), respectively.

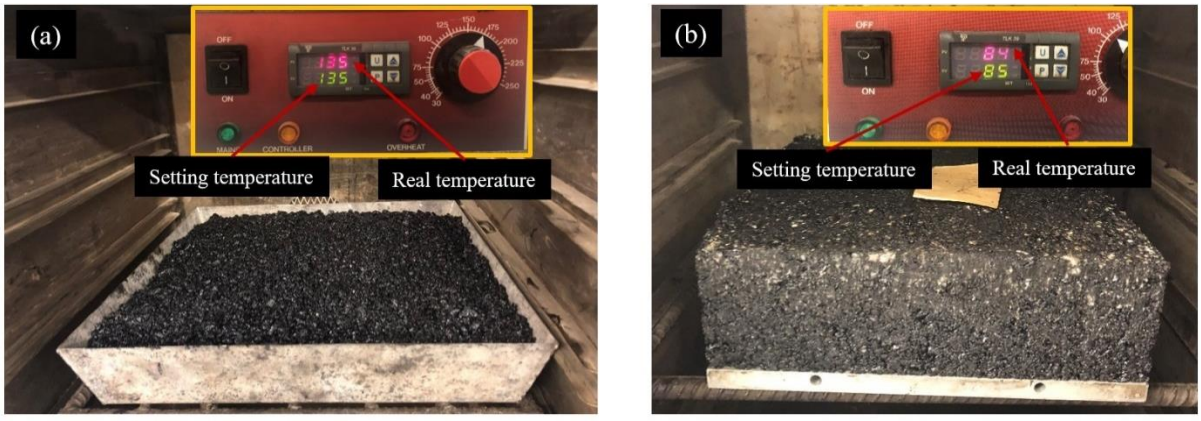

Figure 2: Oven setting and the materials after (a) short-term ageing and (b) long-term ageing.

2.2.2 Two Point Bending (2PB) Fatigue Test

Fatigue tests were carried out using the 2PB equipment. The test consists of applying a continuous sinusoidal waveform at the top of a trapezoidal specimen. To prepare the samples for 2PB, trapezoidal specimens were manufactured from slabs with dimensions: 305 mm length, 305 mm width and 85 mm depth. Twelve specimens were produced from one slab using the process shown in Figure 3 (a). The dimensions required for a 14 mm size DBM are taken from BS EN 12697-24: 2018 [26]. The samples were glued to metal plates using epoxy resin to enable them to be fitted to the test apparatus (see Figure 3(b)). The bottom base is fixed so that the specimen is mounted as a vertical cantilever, allowing a sinusoidal displacement to be applied to the top of the specimen.

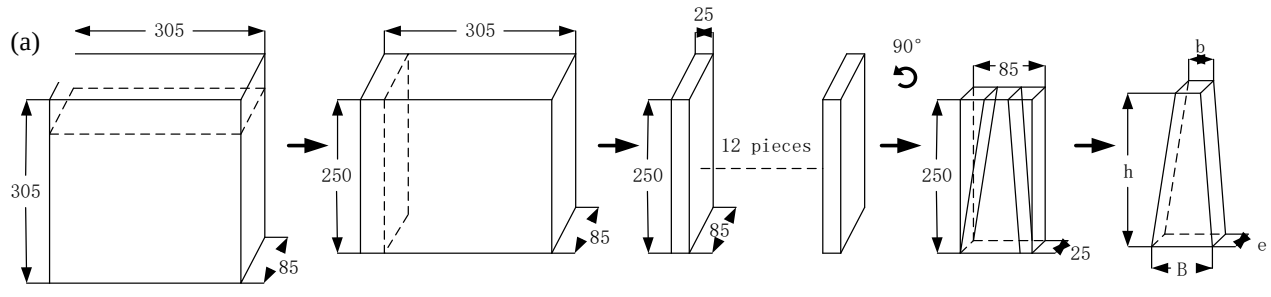

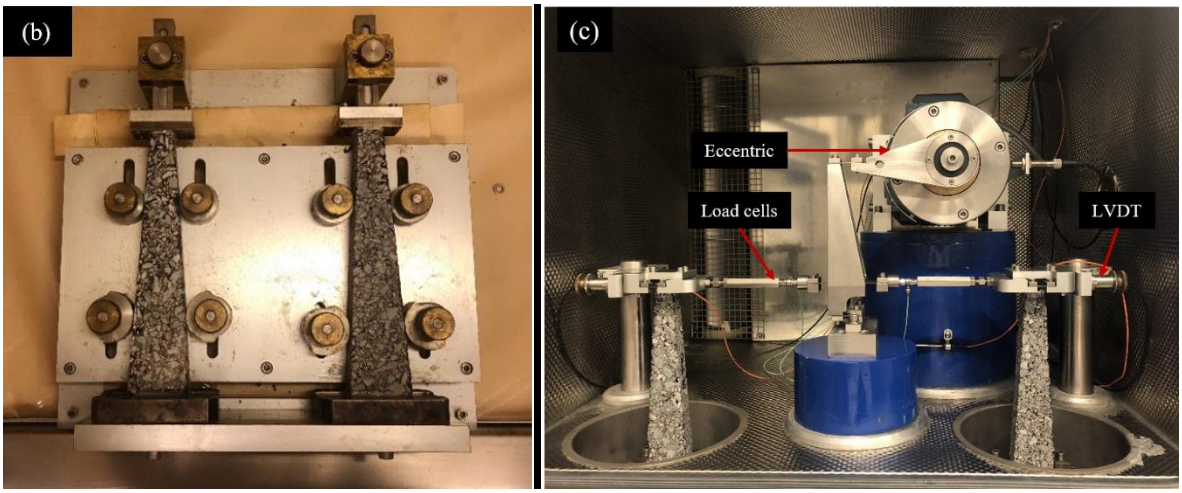

Figure 3: Sample preparation and setting of 2PB: (a) schematic diagram of preparation of trapezoidal specimens; (b) gluing procedure of samples and (c) setting procedure of samples.

The 2PB tests were conducted under strain-controlled mode using sinusoidal loading. The specimens are subjected to different strain levels - 150, 200 and 250 με at different temperatures - 0, 5, 10 and 20 °C at a frequency of 15 Hz. All samples were conditioned for 4 hours before the start of the tests. According to the standard [26], the sample stiffness at the 100th cycle is defined as the initial stiffness. In this study, the failure criteria were studied at different reductions of the initial stiffness value. Therefore, the test was set to stop once the stiffness reach 10% of the initial stiffness value. The equipment tests two specimens at each strain level. Figure 3 (c) shows the test equipment and the samples ready for testing.

2.2.3 Four Point Bending (4PB) Fatigue Test

The 4PB test was applied to prove the applicability of the SCTM in another test method. The test consists of applying a continuous sinusoidal waveform at a constant frequency of 15 Hz at the top of a prismatic specimen by means of two loading points. The specimen is restrained at four points by means of four clamps. Free translation and rotations are allowed at all load and reactions points. Deformation is calculated by means of three Linear Variable Differential Transformers (LVDTs) located at three different points (Figure 4). The beams were tested under strain-controlled mode at a strain level of 270 με. The thermostatic chamber and the loading equipment were set at the test temperature, 10 °C for at least 3 hours prior to the start of the experiment. The fatigue test was conducted according to BS EN 12697-24: 2012.

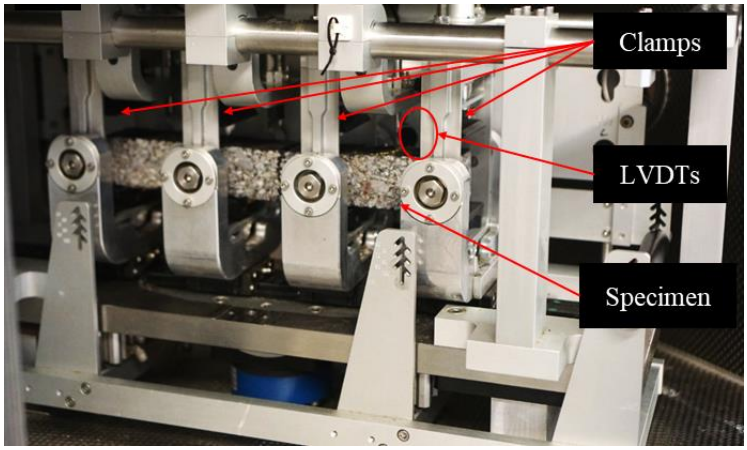

Figure 4: Setup and sketch of 4PB test.

2.2.4 Moisture Damage Tests

The sensitivity test used in this research is that described in BS EN 12697-23:2017 [27]. The vacuum procedure was conducted under a residual pressure of 6.7 ± 0.3 kPa for 30 ± 5 minutes before the specimens were placed in a water bath. A thermostatically controlled water bath is capable of maintaining the prescribed conditioning temperature in the vicinity of the specimens. The bath is equipped with a perforated shelf, placed on spacers above the bottom. The capacity of the bath is such that the test specimens can be stored with the upper surface more than 20 mm below the water surface. The specimens were put in a water bath at 40 ± 2 °C for a period of 72 ± 2 hours, as shown in Figure 5.

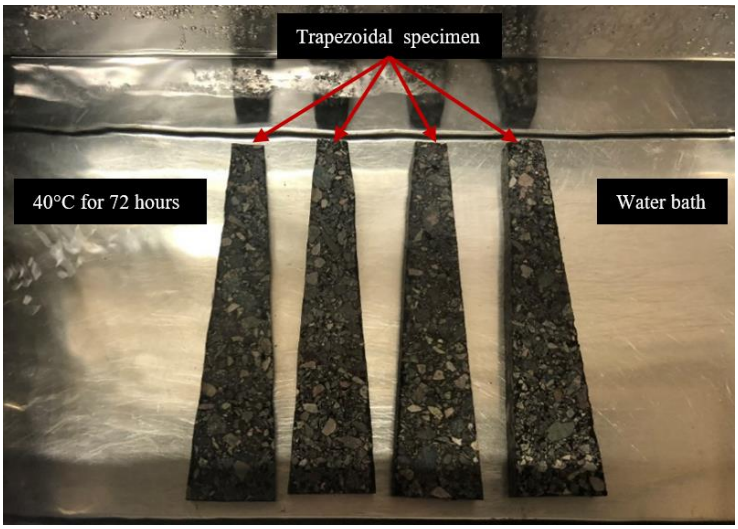

Figure 5: Water bath for moisture conditioning of specimens.

2.3 Stiffness Change Tendency Method (SCTM)

A typical plot of the “S” shape stiffness reduction curve is shown in Figure 6. Four stages are defined by

researchers based on three transition points (P1, P2 and P3), relating to different damage progression [8-9, 28]. Prior to P1, the asphalt stiffness is high and decreases in a relatively stable manner from the initial stiffness. After P1, the reduction in stiffness rapidly increases until the second transition point P2, at P2 the rate of loss of stiffness is maximum. Following P2 the reduction in stiffness decreases and the stiffness approaches zero after P3. In regions III and IV, the road would probably already have failed. The SCTM is developed to model stiffness change and determine transition points.

The typical logistic curves and the base logistic equation are shown in Figure 7; two asymptotes 0 and 1 can be seen. Changing the value of μ shifts the function in the x direction; changing the value of γ impacts the gradient of the function [29]. It can be seen that the shape of the typical curves in Figure 7 are similar to the stiffness reduction curve in Figure 6. Therefore, the logistic model is used to determine the relationship between the log of the stiffness (E) and the log of the number of cycles (N) by transforming the base logistic equation to obtain Equation 1. The constants A, B and C are determined using regression methods in the SAS software. Two asymptotes A1 and A2 can be seen in Figure 8. A1 can be seen to represent the initial stiffness when the sample deformation is highly elastic. A2 represents the stiffness as the number of cycles tends to infinity and the sample fails. The second derivative of the logistic model represents the changing rate of the gradient of the function, therefore it can be used to calculate the exact transition points P1, P2 and P3 [30-31]. These are represented by the maximum, minimum and equilibrium of the second derivative of Equation 1 (lgE"), as shown in Figure 8.

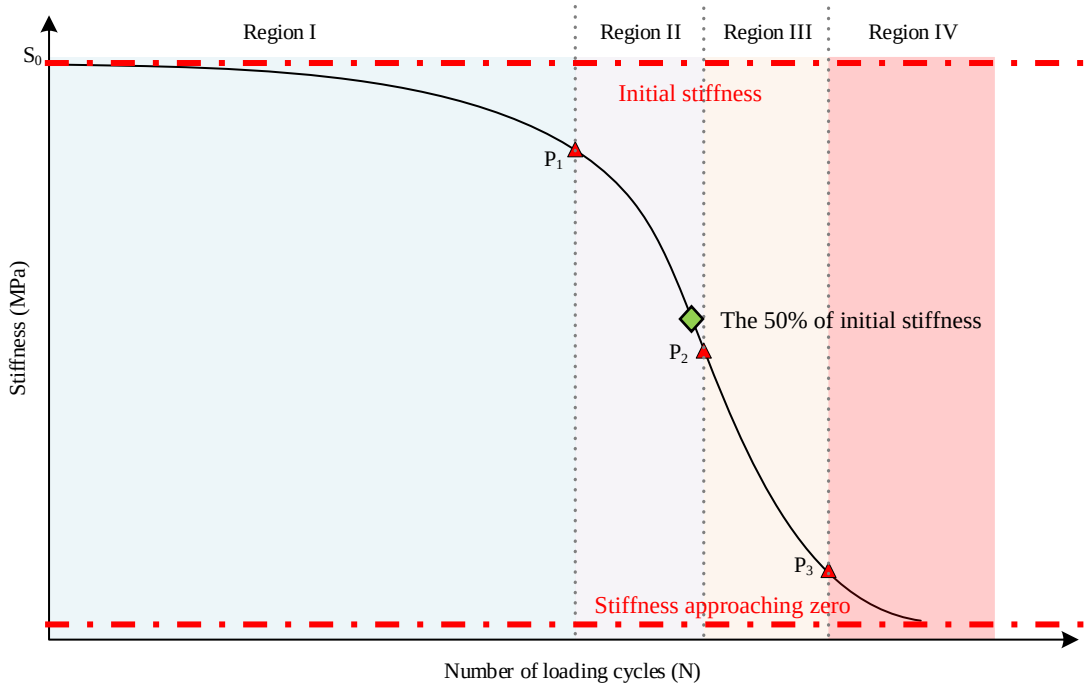

Figure 6: The four regions of a stiffness reduction curve, based on three transition points.

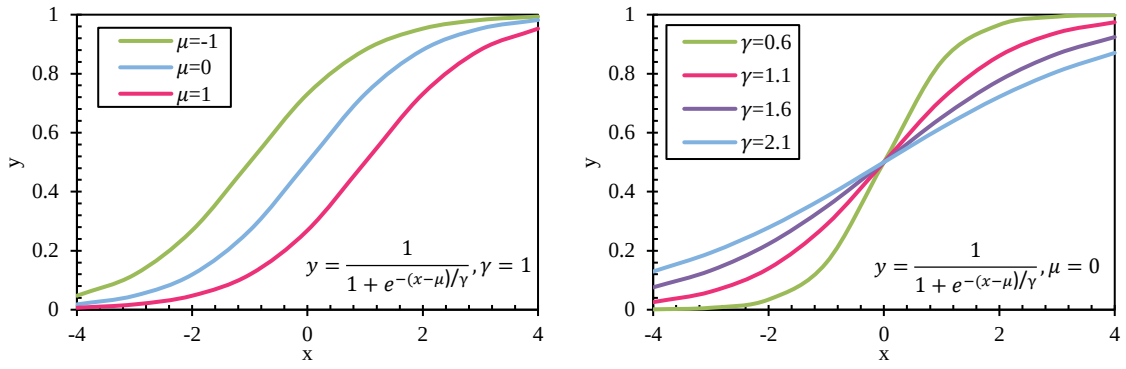

Figure 7: The typical curves of the logistic regression.

$$lgE = \mathrm{A} - \frac{(lgN)^B}{C^B + (lgN)^B}, \quad (1)$$

where E is the stiffness (MPa), N is the number of cycles, A, B and C are constants.

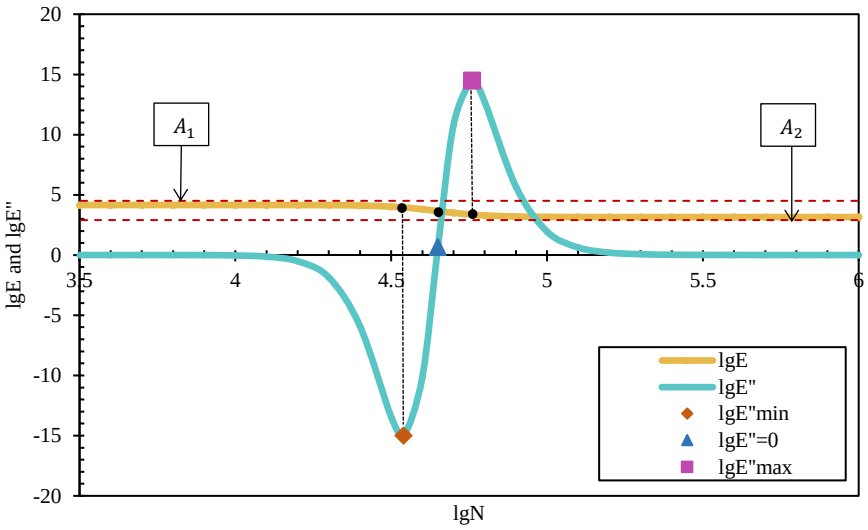

Figure 8: Fitting logistic equation and it's the second derivative.

2.4 Energy-based Approaches

The ER and RDEC approaches are applied to validate the results obtained from the SCTM. The data collected at 10 ℃ under 150 με is chosen as an example; the phenomenological stiffness (E) versus the number of cycles (N) on logarithmic scales is applied to show the position of N_{f50} as a comparison (Figure 12).

The basis of the ER and RDEC approaches is to calculate the dissipated energy cycle per unit volume (W), shown in Equation 2 [32]. It is known that an asphalt mixture is a viscoelastic material, therefore its stress-strain curve under repeated loading is non-linear. The loading and unloading paths do not overlap, instead they form loops,

known as hysteresis loops [3]. The area of the hysteresis loop is defined as the dissipated energy [2].

$$W = \pi\sigma\varepsilon \sin\varphi, \tag{2}$$

where σ is the stress level in each cycle; ε is the strain level in each cycle and φ is the phase angle in each cycle.

For asphalt mixtures under strain-controlled loading mode, the dissipated energy evolution will follow three stages connected by two transitions [17], as shown in Figure 9. The first stage is considered as a no damage or minimal damage region. The ER approach was used to calculate the value of the first transition point (N_1). N_1, is defined as the point of crack initiation [4], at this point the ER changes from a good linear relationship to a significantly noisier relationship, as shown in Figure 10. ER is the ratio between the initial dissipated energy (W_0) multiplied by the cycle number (n) and the dissipated energy in the n^{th} cycle (W_n), shown in Equation 3 [8].

$$ER = \frac{nW_0}{W_n} = \frac{n(\pi\sigma_0\varepsilon_0 \sin\varphi_0)}{(\pi\sigma_n\varepsilon_n \sin\varphi_n)}, \tag{3}$$

where σ_0, ε_0 and φ_0 are stress, strain and phase angle in the initial cycle and σ_n, ε_n and φ_n are stress, strain and phase angle in the nth cycle.

After the first transition point, the dissipated energy curve enters the second stage (the plateau stage) where the dissipated energy drops at a relatively constant rate, until the third stage where the dissipated energy curve has a significantly different slope (Figure 9). The transition point between the second and the third stage is related to macrocrack propagation [11]. Ghuzlan and Carpenter [11] used the RDEC approach to define N_{fm} as the macroscopic failure, according to Figure 11 and Equation 4. The RDEC approach was refined by Shen and Carpenter [17] to calculate N_{fm}, the cycle number corresponding to the maximum ΔA (Equations 5-7).

$$\text{RDEC} = \frac{W_{n+1} - W_n}{W_n}, \tag{4}$$

where RDEC is the ratio of the dissipated energy change per load cycle, W_n is the dissipated energy produced in load cycle n and W_{n+1} is the dissipated energy produced in load cycle $n+1$.

$$\Delta\text{A} = |AT - SDE|, \tag{5}$$

$$\text{SDE} = \sum_{0}^{n} DE, \tag{6}$$

$$AT = \frac{(DE_0 + DE_i) \times n}{2}, \tag{7}$$

where n is the cycle number, DE_0 is the initial dissipated energy and DE_i is the dissipated energy at cycle i. SDE is the area under the dissipated energy curve, AT is the trapezoidal area and ΔA is the difference between SDE and AT, as shown in Figure 9.

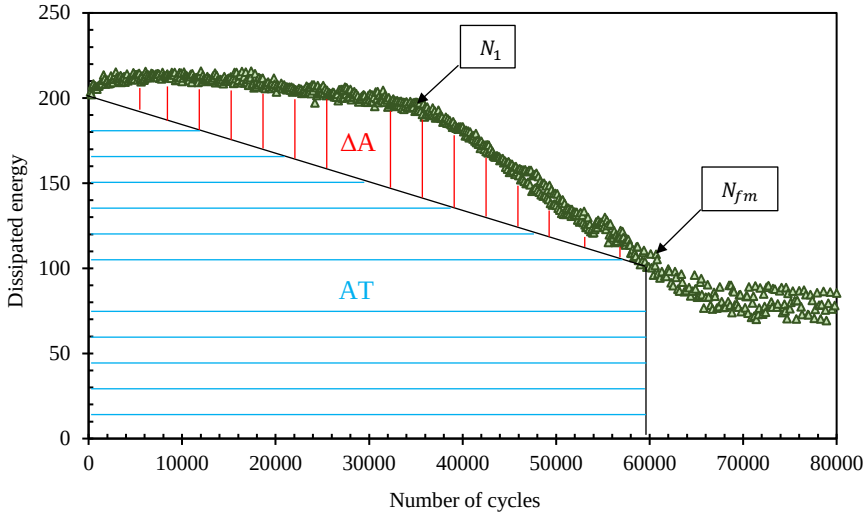

Figure 9: Dissipated energy versus number of load cycles (10°C, 150με).

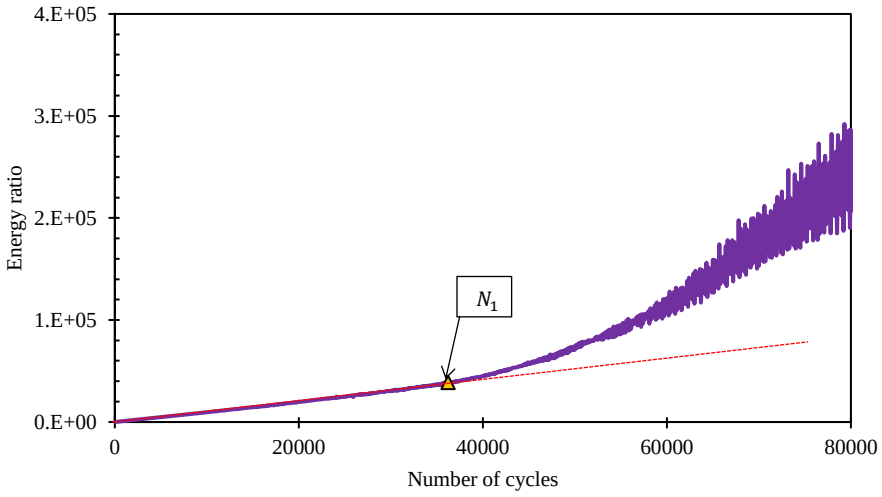

Figure 10: ER versus number of load cycles (10 °C,150 με).

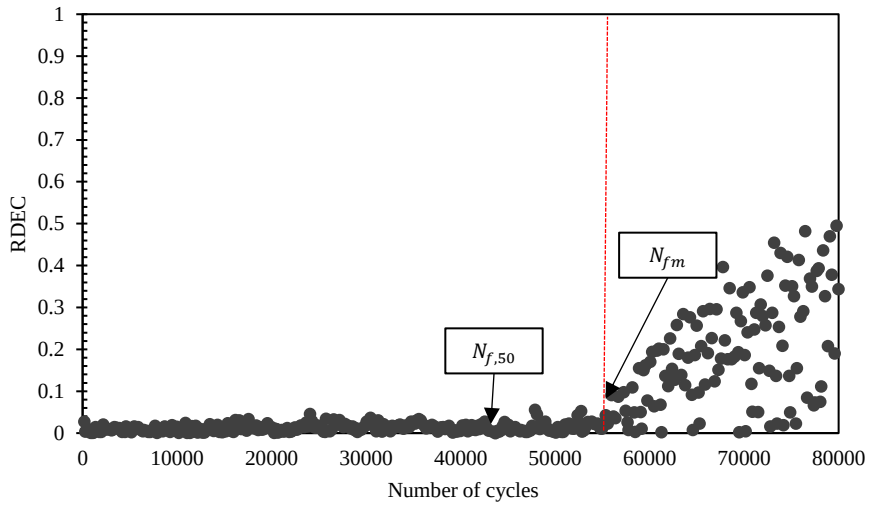

Figure 11: RDEC versus number of load cycles (10 °C, 150 με).

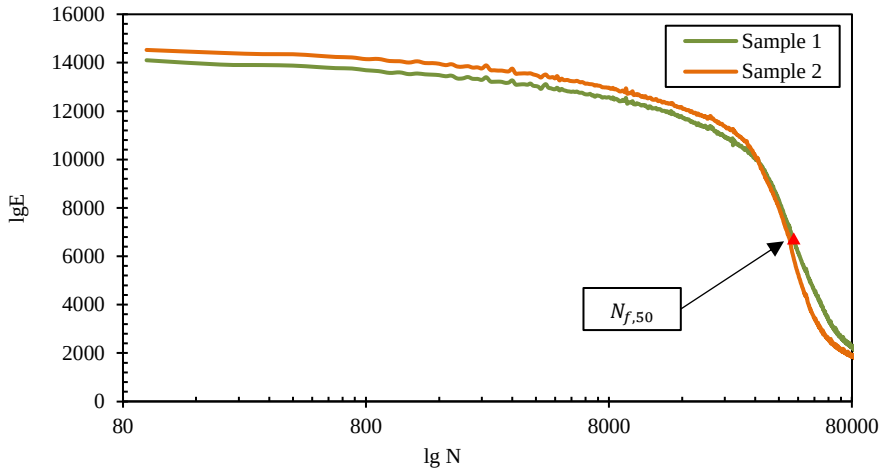

Figure 12: lgE versus lgN (10 °C, 150 με).

3 Results and Discussion

3.1 Stiffness Change Tendency Method (SCTM)

The test design mainly considers the applicability of the SCTM for different conditions, including aged and moisture damaged, different test methods, different test temperatures and strains, and different types of mixtures, as shown in Table 2. Samples were subjected to four repeated tests per test condition; with the results being averaged. Based on the data points (shown in blue in Figures 13-14) obtained from the tests, a logistical model of the form in Equation 1 is fitted to the data (shown in red Figures 13-14) with the constants A, B and C being determined using SAS software. The constants determined using the SAS software are shown in Table 2 alongside their R^2 values. The R^2 values show that in all cases there is good agreement between the laboratory data and the fitted logistic model, confirming that the logistic model it is a suitable model to model the stiffness reduction curve. Visual comparison of Figures 13-14 shows the equation does not quite match at the beginning of some

curves. The initial drop in stiffness at the beginning of the stiffness reduction curves, which may be partly due to temperature increase, are not considered by the equation. The derivatives of the logistic model are shown in Table 3 alongside the Stiffness Ratio ($SR = E/S_0$). This illustrates that the stiffness ratio at the three transition points is similar across all samples. P1 occurs between 48% and 68% of the initial stiffness (S_0). The stiffness ratio at P2 ranges between 22% and 35% of S_0, and at P3 ranges between 12% and 17% of S_0.

Based on the fitted logistic model, three transition points (P1, P2 & P3 as shown in Figures 13-14) associated with fatigue progression were determined to characterise the different fatigue damage stages. The stiffness reduction in region I (prior to P1) is observed to be slow. The stiffness drops sharply during region II (between P1 and P2), after region II the rate of loss of stiffness decreases until P3.

The values of the stiffness and corresponding number of cycles at each failure point is affected by factors such as temperature, ageing and moisture damage. Seen from Table 3 (sample sets 1-4), under the same strain level, at the higher the temperature, the later the failure point occurs. E_{p1}, E_{p2} and E_{p3} happen at 52%, 22% and 12% of S_0 at 20℃, respectively, while at 0 ℃, they happen at 68%, 31% and 17% of S_0, respectively. Similarly, seen from Figures 13 (a) and (b), the higher the temperature, the greater the corresponding number of cycles at the failure point. N_{p1}, N_{p2} and N_{p3} at 20 ℃ are 55000, 72500 and 93400, while at 0℃, these are 22400, 41100 and 72500, respectively. Figures 13 (c) and (d) show that fatigue performance deteriorates after ageing and moisture damage compared to undamaged condition. Moisture damage has a greater impact on fatigue performance with aged samples experiencing 35500 cycles while moisture damage samples experienced 19100 cycles at 15% initial stiffness. However, the value of P1 for the moisture damaged samples occurs at a lower stiffness value compared to the aged samples.

The fitting results are presented in Figure 14 alongside the data obtained for the 4PB tests. As with the 2PB, a good likeness is observed and the R^2 values of all fitted models are close to unity, demonstrating that the SCTM is applicable to be used to model stiffness development of different asphalt mixtures and different test methods. The 4PB fatigue tests of the three bituminous mixtures in Figure 14 were stopped at 20% of the initial stiffness of the samples, however, the value of N_{P3} can still be predicted using the SCTM. This proves that the SCTM is able to predict fatigue failure points and remaining fatigue life as long as part of the fatigue test data is known, removing the need for time intensive laboratory testing.

Table 2: Fitting results for the Logistic model.

Sample set	Test Method	Bitumen	Mixture type	Temperature (℃)	Strain (με)	Condition	Logistic model constants			R^2
							A	B	C	
1	2PB	Pen 40/60	DBM-14	0	200	unaged	4.32	23.55	4.63	0.94
2	2PB	Pen 40/60	DBM-14	5	200	unaged	4.23	46.4	4.27	0.88

3	2PB	Pen 40/60	DBM-14	10	200	unaged	4.15	57.57	4.65	0.86
4	2PB	Pen 40/60	DBM-14	20	200	unaged	3.77	56.1	4.86	0.82
5	2PB	Pen 40/60	DBM-14	10	150	unaged	4.1	37.96	4.77	0.91
6	2PB	Pen 40/60	DBM-14	10	250	unaged	4	57.41	4.33	0.80
7	2PB	Pen 40/60	DBM-14	10	200	moisture damaged	4.06	39.91	4.15	0.86
8	2PB	Pen 40/60	DBM-14	10	200	aged	4.18	27.74	4.36	0.88
9	4PB	Pen 40/60	DEM-10	10	270	unaged	4.06	19.10	3.90	0.88
10	4PB	CRMB	DEM-10	10	270	unaged	4.11	16.42	3.85	0.87
11	4PB	Pen 40/60	SMA-10	10	270	unaged	4.08	22.00	3.93	0.89

Table 3: Results of second derivative function and the corresponding stiffness ratio (SR).

Sample set	lgE''_{min}	$lgE''=0$	lgE''_{max}	E_{p1} (MPa)	E_{p2} (MPa)	E_{p3} (MPa)	S_0 (MPa)	SR $_{p1}$	SR $_{p2}$	SR $_{p3}$
1	4.35	4.61	4.86	14447	6632	3686	21099	68%	31%	17%
2	4.15	4.27	4.38	11189	5015	2825	18868	59%	27%	15%
3	4.54	4.65	4.76	9367	4225	2215	17105	55%	25%	13%
4	4.74	4.86	4.97	3965	1700	935	7633	52%	22%	12%
5	4.6	4.76	4.93	8340	4333	2039	14102	59%	31%	15%
6	4.23	4.33	4.43	6512	3608	1646	13667	48%	26%	12%
7	4.00	4.14	4.28	10900	4395	2592	17126	55%	26%	14%
8	4.15	4.35	4.55	7727	3654	1933	13931	64%	26%	15%
9	3.59	3.87	4.15	7623	4327	1986	12234	62%	35%	16%
10	3.52	3.83	4.14	8018	4169	2202	13343	60%	31%	17%
11	3.68	3.91	4.15	8196	4287	2063	12649	65%	34%	16%

(a)

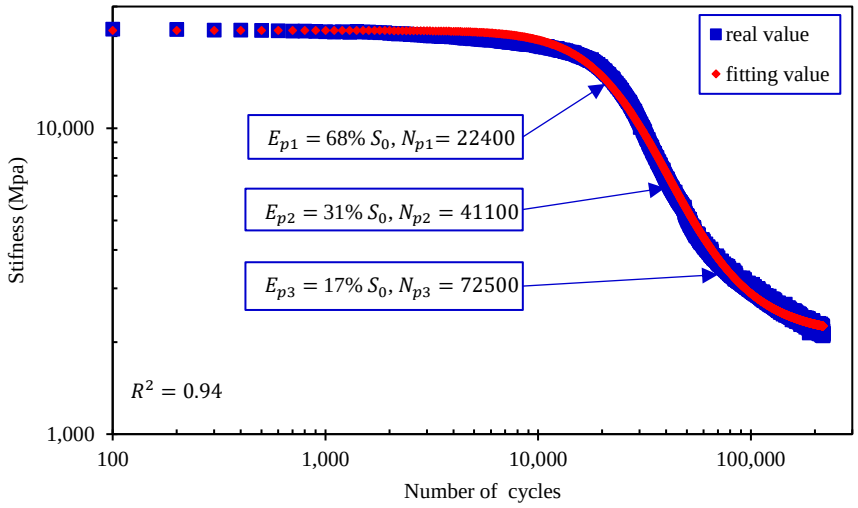
real value
fitting value
$E_{p1} = 68\%\ S_0,\ N_{p1} = 22400$
$E_{p2} = 31\%\ S_0,\ N_{p2} = 41100$
$E_{p3} = 17\%\ S_0,\ N_{p3} = 72500$
$R^2 = 0.94$
10,000
1,000
100
1,000
10,000
100,000
Stifness (Mpa)
Number of cycles

(b)

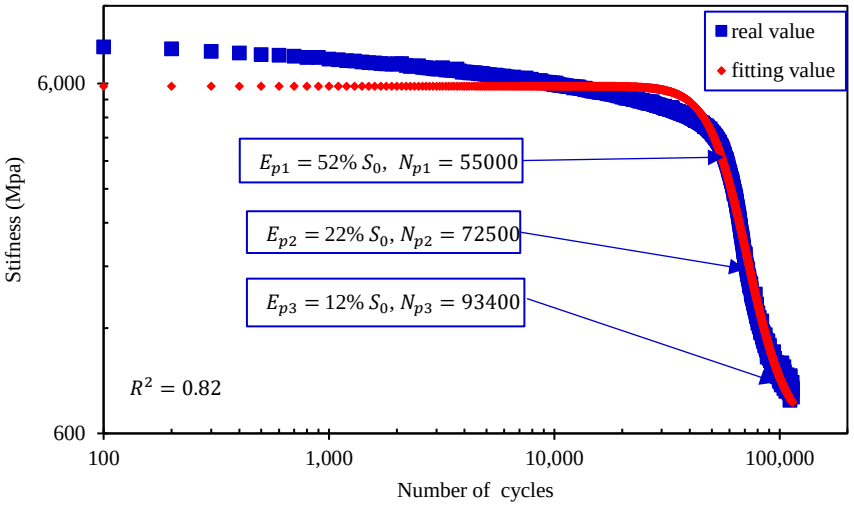
real value
fitting value
$E_{p1} = 52\%\ S_0,\ N_{p1} = 55000$
$E_{p2} = 22\%\ S_0,\ N_{p2} = 72500$
$E_{p3} = 12\%\ S_0,\ N_{p3} = 93400$
$R^2 = 0.82$
6,000
600
100
1,000
10,000
100,000
Stifness (Mpa)
Number of cycles

(c)

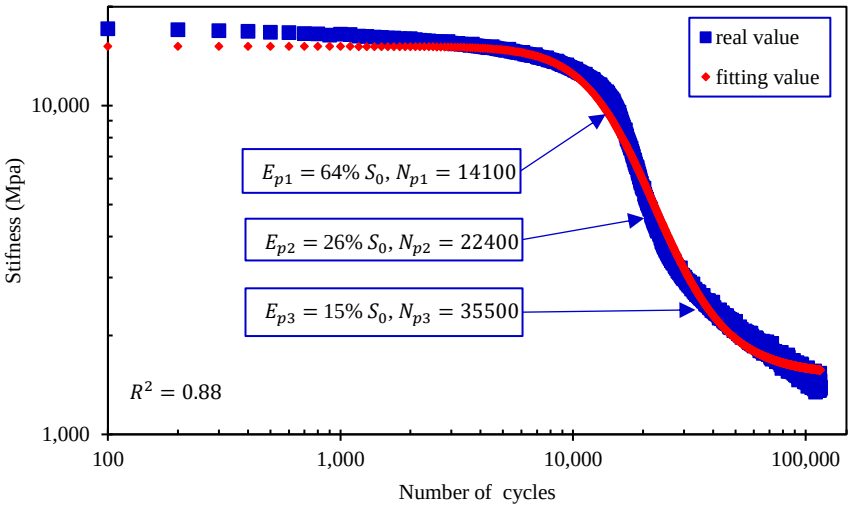
real value
fitting value
$E_{p1} = 64\%\ S_0,\ N_{p1} = 14100$
$E_{p2} = 26\%\ S_0,\ N_{p2} = 22400$
$E_{p3} = 15\%\ S_0,\ N_{p3} = 35500$
$R^2 = 0.88$
10,000
1,000
100
1,000
10,000
100,000
Stifness (Mpa)
Number of cycles

(d)

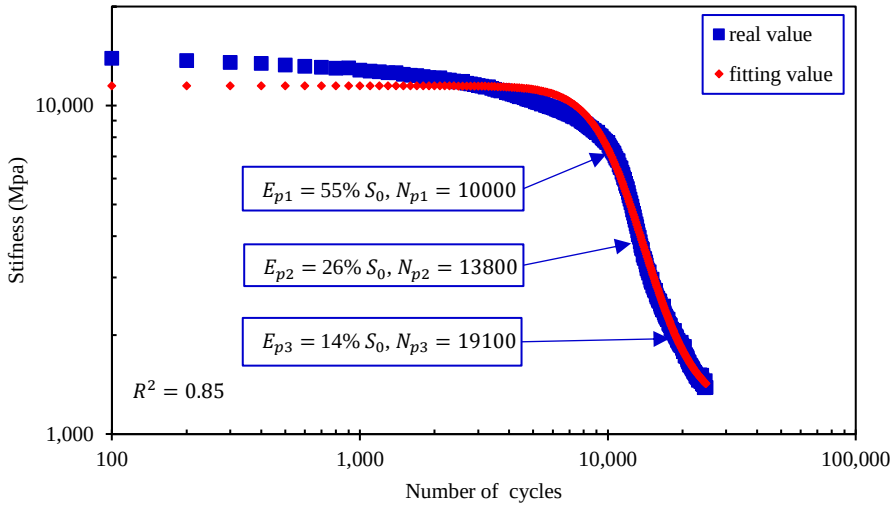

270 Figure 13: Fitting results under different temperatures, strains and conditions of 2PB tests: (a) 0 ℃ and 200 με;
271 (b) 20 ℃ and 200 με; (c) 10 ℃ and 200 με aged; (d) 10 ℃ and 200 με moisture damaged.

(a)

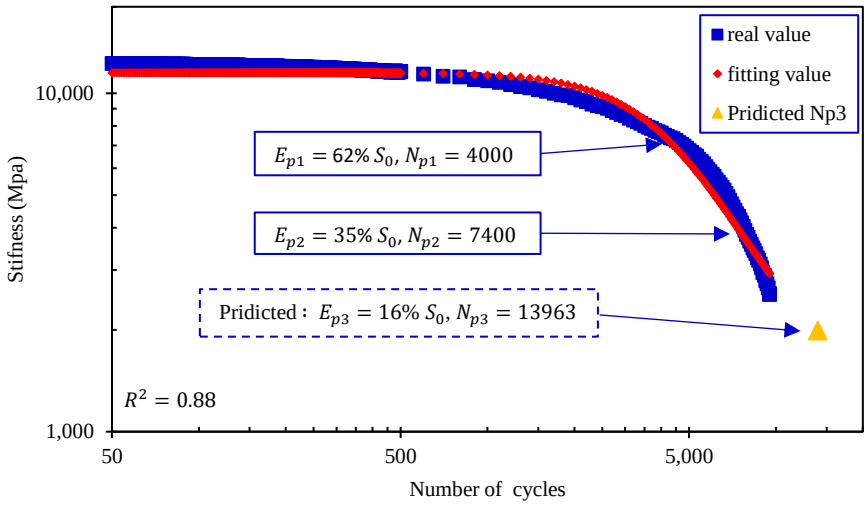

(b)

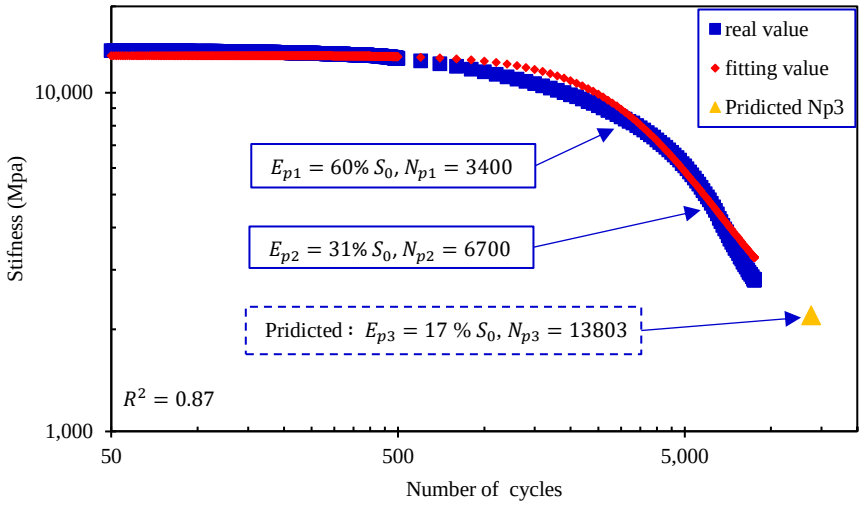

(c)

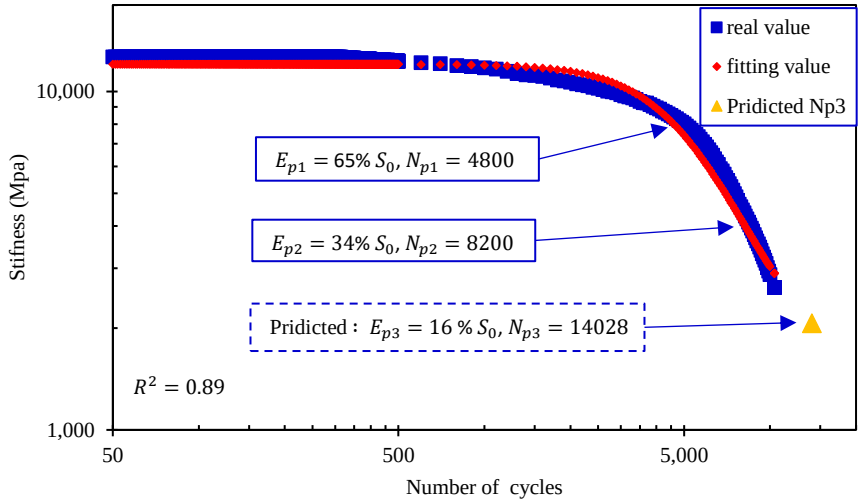

Figure 14: Fitting results of different asphalt mixtures at 10 ℃ under 270 με of 4PB tests (a) DBM-14+Pen40/60; (b) DBM-10+ CRMB; (c) SMA-10+Pen40/60.

Unlike the traditional 50% initial stiffness, the transition point happens randomly in the stiffness reduction curve, therefore, it is necessary to evaluate the fatigue performance with regards to the unit stiffness loss. The quotient of the number of cycles and the stiffness loss, $\Omega = \frac{N}{(S_0 - E)}$, was calculated to determine the number of cycles lost per unit stiffness. In other words, Ω expresses how easily stiffness is lost and can be used to evaluate fatigue performance; the more cycles required for a unit stiffness loss, the better the fatigue performance. As shown in the Figure 15, for most sample sets, Ω_{p2} is the smallest, which indicates that stiffness loss is greater at P2, the stiffness reduction curve also shows that the stiffness decreases quickest near P2. Generally, Ω decreased as the temperature increased and the strain decreased. For 2PB tests, fatigue performance under 200 με at 20 ℃ is the best as Ω is the largest, whereas fatigue performance after moisture damage is the worst and has the smallest Ω value. Ω value of 4PB tests are smaller than that of 2PB tests, fatigue performance of SMA-10+Pen40/60 is the best as Ω is the largest.

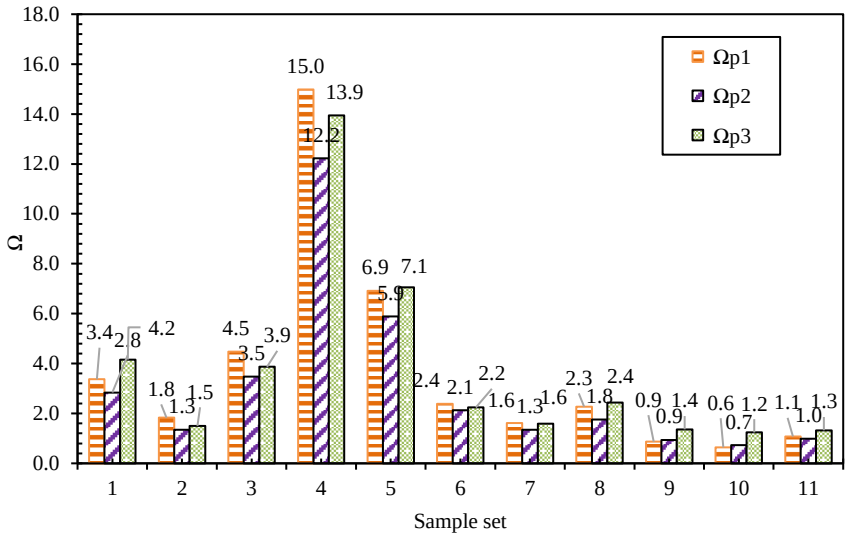

Figure 15: The number of cycles with respect to the stiffness loss, Ω, at P1, P2 and P3.

3.2 Energy-based Fatigue Failure Criteria

3.2.1 Dissipated Energy Approach

Hysteresis loops were calculated to explore the energy change law for different number of cycles in a strain-controlled mode. The damage accumulates and the dissipated energy decreases as the number of loading cycles is increased. The first stage is the no damage or minimal damage region, during which the material's stress-strain hysteresis loop remains similar and there is no apparent change in dissipated energy as seen in Figure 16a. In the second stage, the dissipated energy steadily decreases, which is reflected in the clockwise movement and decrease in area of the stress-strain hysteresis loop (Figure 16b). Most fatigue failure criteria are defined at this stage as it is where macro damage happens. In the third stage, the change in dissipated energy (the stress-strain hysteresis loop) once again becomes minimal; however the area of the stress-strain hysteresis loop decreased significantly compared to the stage 1 (Figure 16c).

(a)

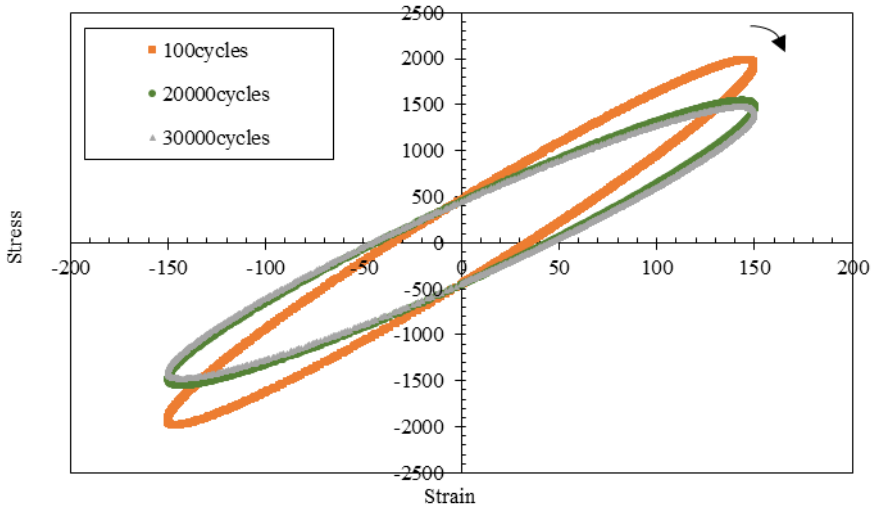

(b)

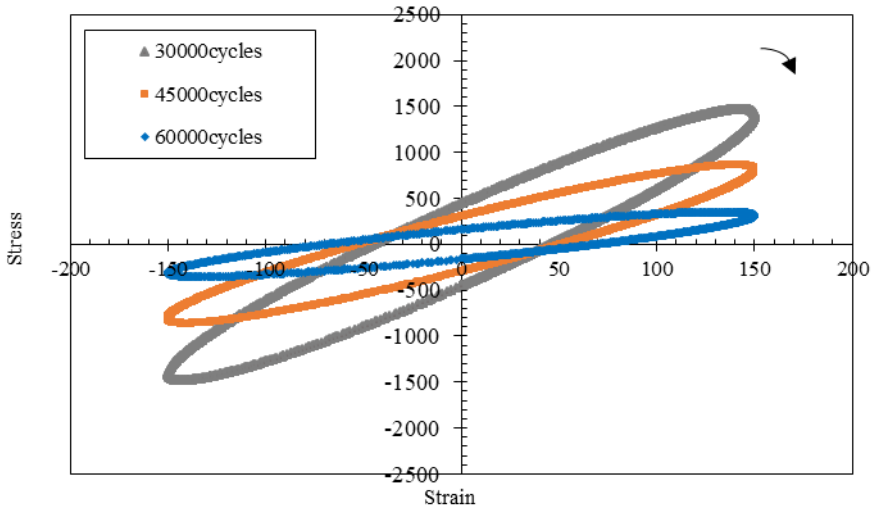

(c)

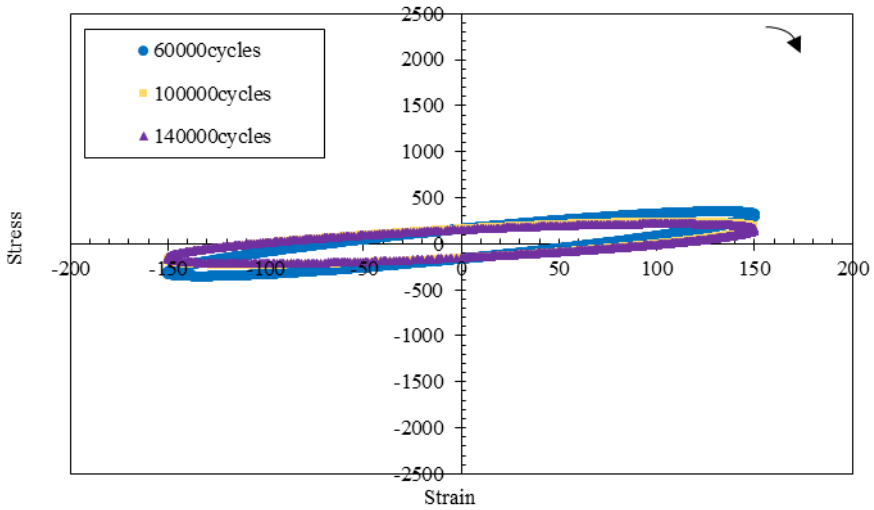

298 Figure 16: Stress-strain hysteresis loops change (10 ℃, 150 με) for controlled strain 2PB test: (a) first stage; (b)
299 second stage and (c) third stage.

3.2.2 Energy Ratio (ER) Approach

Seen in the plot of ER versus number of cycles in the strain-controlled mode (Figure 17), the ER is initially a straight line with a rapid increase after a given number of cycles. N_1 is the inflection point where the ER curve deviates from the linear section (undamaged line in Figure 17). The value of N_1 is affected by factors including temperature, strain, ageing and moisture damage. It can be seen from Figure 17a-c that N_1 generally increases as the temperature increases and decreases with strain increase. Ageing and moisture damage caused different reduction rates of N_1, but the impact of moisture damage is more significant. Figure 17d shows ER versus number of load cycles for controlled strain 4PB test of different mixtures. The N_1 of SMA-10+ Pen40/60 is the largest whereas the N_1 of DBM-10+ CRMB is the smallest, showing that the value of N_1 is also affected by the bitumen type and mixture type. N_1 calculated under all conditions gave a similar undamaged control line thereby confirming that the control line of *ER* vs *N* curves is independent of all the factors investigated.

(a)

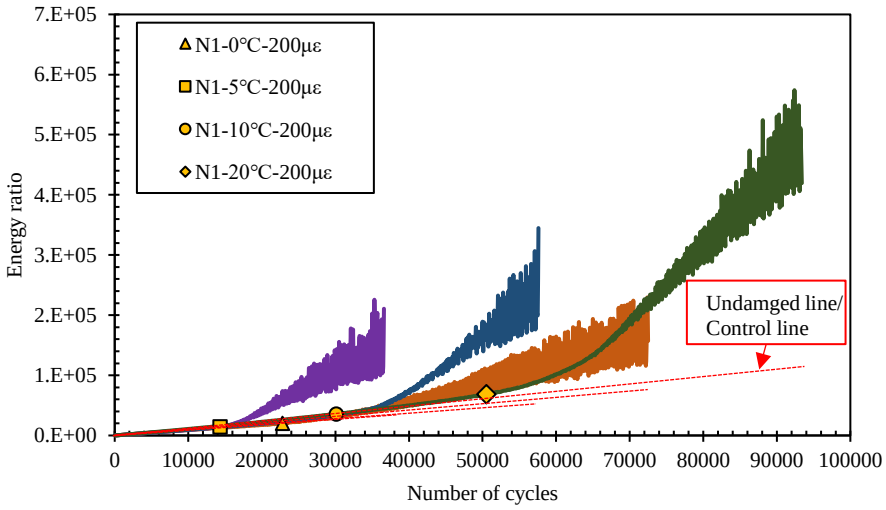

(b)

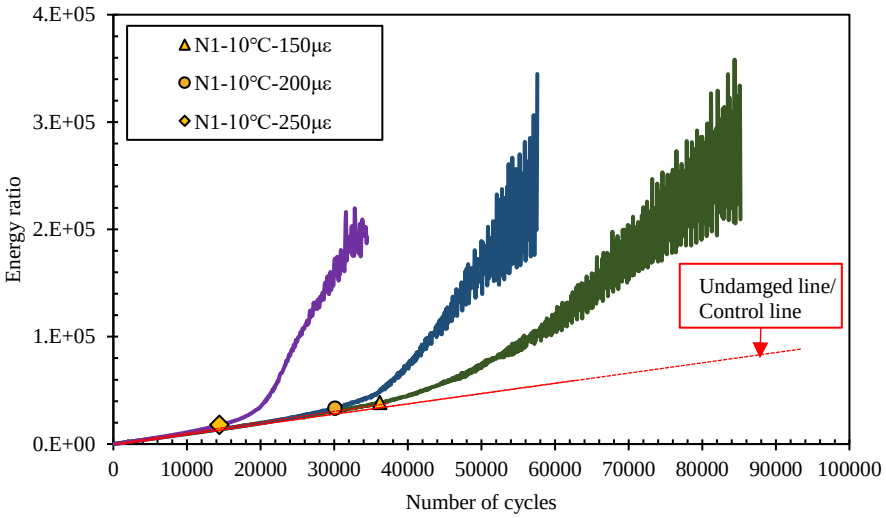

(c)

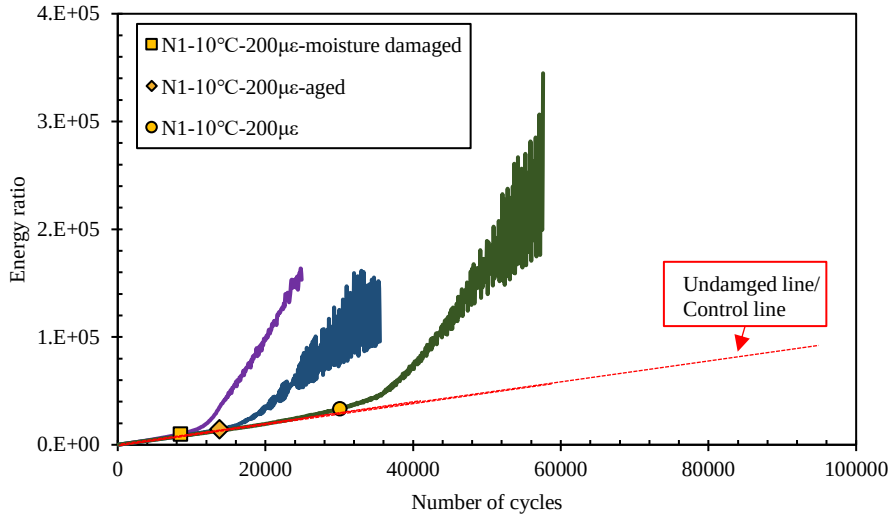

(d)

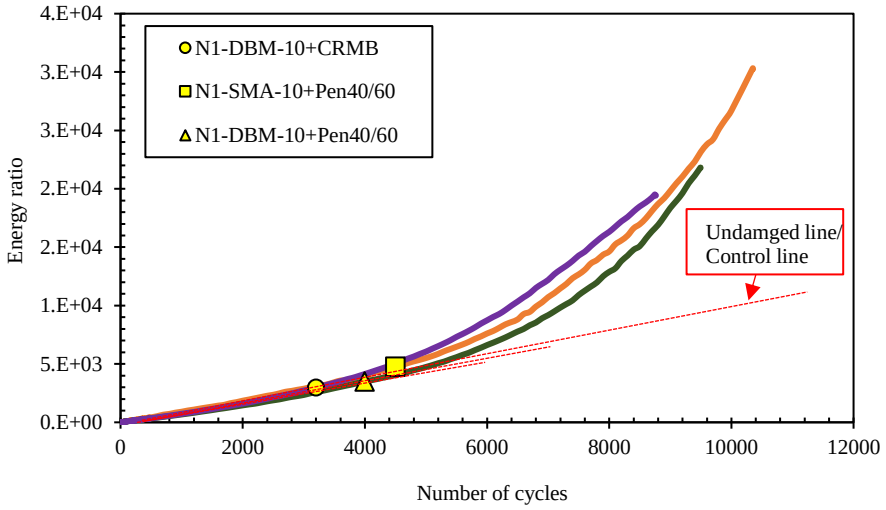

311 Figure 17: Energy ratio versus number of load cycles for controlled strain 2PB test: (a) at different temperatures;
312 (b) under different strains; (c) under different conditions; and for 4PB test: (d) of different mixtures.

313 3.2.3 Ratio of Dissipated Energy Change (RDEC) Approach

314 The results of the second transition point (N_{fm}) are shown in Figure 18. Under strain-controlled loading mode,
315 the area ΔA is initially very small but increases with loading cycles. There is a point where the area ΔA is
316 maximised and this point corresponds to N_{fm}, where macroscopic failure occurs, after which the area ΔA
317 decreases. The value of N_{fm} is also affected by the factors in the same way as N_1, it generally increases as the
318 temperature increases and decreases with strain increase. Ageing and moisture damage also causes the decrease
319 in N_{fm}, where the impact of moisture damage is more significant. The value of N_{fm} is also affected by the bitumen
320 type and mixture type. Unlike N_1, the dissipated energy decline rate at N_{fm} is maximum. At this point cracks are
321 propagating rapidly, which is considered to be the true point of failure.

(a)

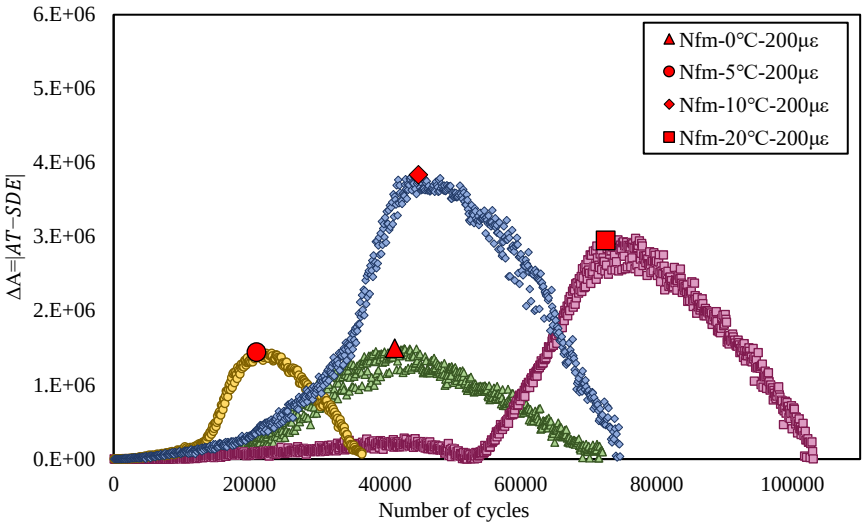
6.E+06
5.E+06
4.E+06
3.E+06
2.E+06
1.E+06
0.E+00
ΔA=|AT−SDE|
0
20000
40000
60000
80000
100000
Number of cycles
Nfm-0°C-200με
Nfm-5°C-200με
Nfm-10°C-200με
Nfm-20°C-200με

(b)

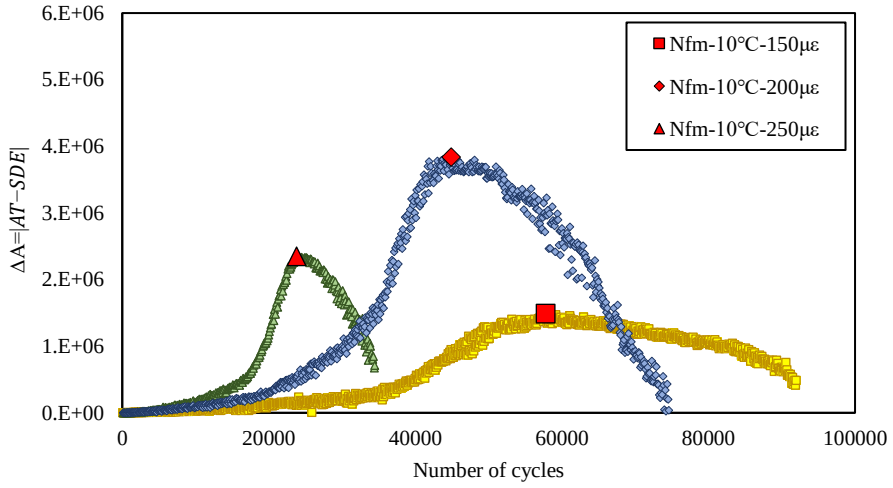
6.E+06
5.E+06
4.E+06
3.E+06
2.E+06
1.E+06
0.E+00
ΔA=|AT−SDE|
0
20000
40000
60000
80000
100000
Number of cycles
Nfm-10°C-150με
Nfm-10°C-200με
Nfm-10°C-250με

(c)

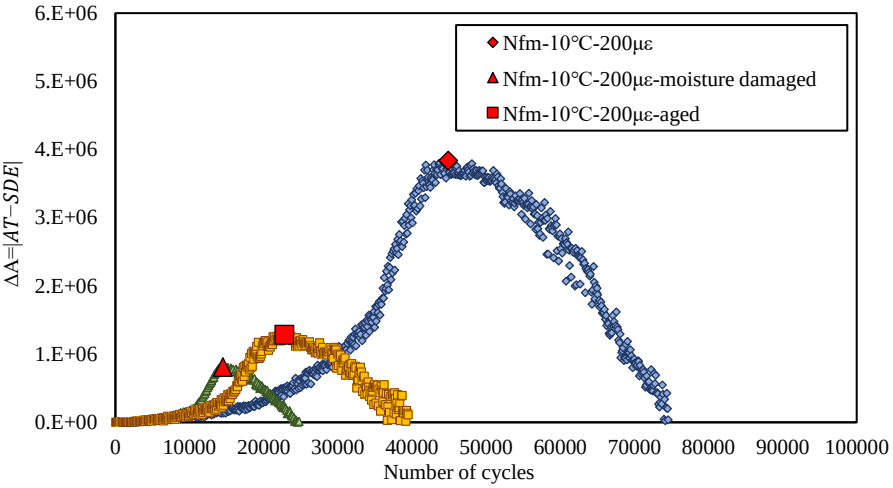
6.E+06
5.E+06
4.E+06
3.E+06
2.E+06
1.E+06
0.E+00
ΔA=|AT−SDE|
0
10000
20000
30000
40000
50000
60000
70000
80000
90000
100000
Number of cycles
Nfm-10°C-200με
Nfm-10°C-200με-moisture damaged
Nfm-10°C-200με-aged

(d)

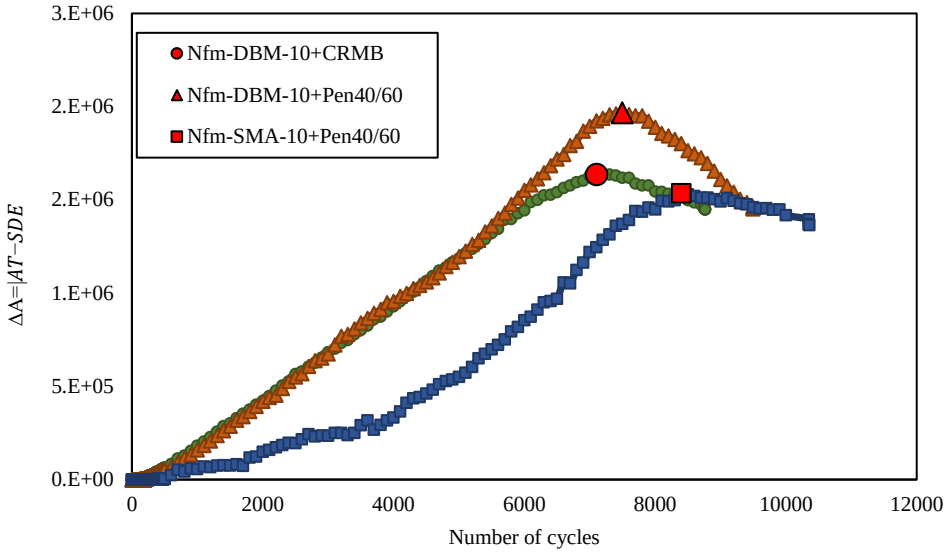

Figure 18: ΔA versus number of cycles for controlled strain 2PB test: (a) At different temperatures, (b) Under different strains; (c) Under different conditions and for 4PB test: (d) of different mixtures.

3.3 Validation of the SCTM

This research compares the number of loading cycles at P1 and P2 in the SCTM with the values of N_1 and N_{fm} obtained from two different energy-based methods (the ER method and the RDEC method). The results obtained from the two different energy-based methods and SCTM are shown in Figure 19. The figure shows that differences between P1 and micro cracking point are generally greater than those between P2 and the macro-crack generation point. For different conditions, including aged and moisture damaged, different test methods, different test temperatures and strains, and different types of mixtures, the results calculated by the SCTM are similar to those calculated by the energy-based methods. The one-way analysis of variance (ANOVA) is applied to show the difference between the proposed method and the two energy methods. The results indicate that there are no statistically significant differences between the SCTM and the two energy methods, as determined by one-way ANOVA ($F < F_{crit}$, P-value > 0.05 for all sample sets), confirming that the SCTM is indeed appropriate to model stiffness loss and be used as a means to calculate the fatigue failure criteria. P1 can be viewed as the number of cycles to micro-crack initiation and propagation. The region prior to P1 is the micro-crack formation region. P2 can be defined as the macro-crack generation point; the true failure point is at P2.

(a)

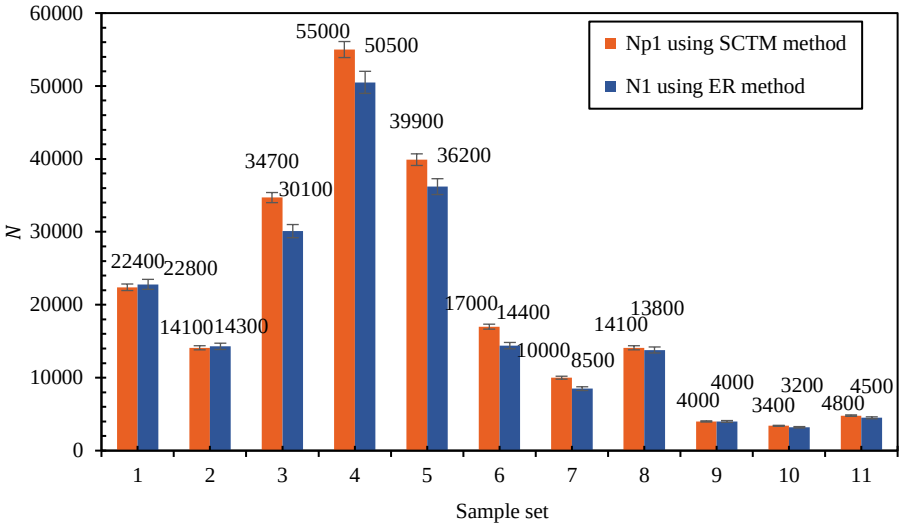

(b)

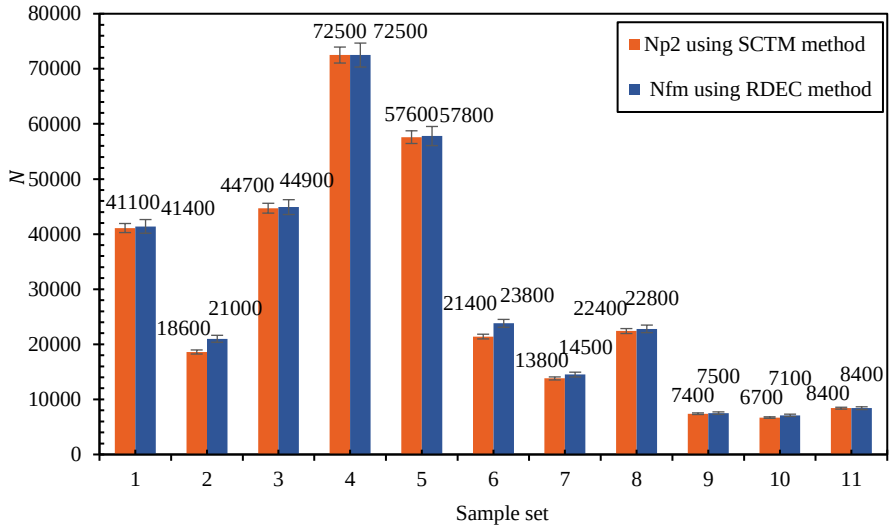

Figure 19: Comparison of fatigue failure criteria gained from different methods: (a)N_{p1} and N_1 ; and (b) N_{p2} and N_{fm}.

4 Conclusions

In this paper a stiffness change tendency method (SCTM) is proposed to determine transition points in lgE v lgN curves. These transition points are compared to the values of N_1 and N_{fm} calculated using energy-based methods. The main conclusions of the study are as follows:

1. There is good agreement between the laboratory data and the proposed logistic model, confirming that the logistic model is a good approximation to model stiffness development.

2. It is illustrated that the stiffness ratio at the three transition points are similar across all samples. P1 occurs between 48% and 68% of the initial stiffness (S_0). The stiffness ratio at P2 ranges between 22% and 31% of S_0, and at P3 ranges between 12% and 17% of S_0. Under the same strain level, the higher the

temperature, the later the failure point occurs.

3. The quotient of cycles with the respect to the stiffness loss, **Ω**, at the different fatigue failure points can effectively evaluate the fatigue performance of asphalt concrete at different damage stages; it is affected by factors, such as temperature, strain level, ageing and moisture damage.

4. The number of loading cycles at the transition points P1 and P2 (N_{p1} and N_{p2}) in the SCTM have a good likeness with the values of N_1 and N_{fm} obtained in the energy-based methods. P1 can be viewed as the number of cycles to micro-crack initiation and propagation. The region prior to P1 is the micro-crack formation region. P2 can be defined as the macro-crack generation point; the true failure point is at P2.

5. The SCTM is feasible to be used to model stiffness development of different asphalt mixtures and test methods. The SCTM also has benefits of predicting fatigue failure points and remaining fatigue life as long as part of fatigue test data are known.

The SCTM combines the benefits of both approaches (phenomenological and energy-based). It provides a promising method of modelling stiffness development, determining the fatigue failure points to characterise different fatigue damage stages, evaluating fatigue performance, as well as, relating the fatigue failure points to different fatigue cracking processes, which could all be useful in a simulation of pavement deterioration in the future.

5 Funding

The funding for this project was provided by Faculty of Engineering Research Excellence PhD Scholarship.

6 Conflicts of Interest

The authors declare no conflict of interest.

References

[1] Miner, M., Cumulative fatigue damage. Journal of applied mechanics, 1945. 12(3): p. A159-A164.

[2] Kim, Y.-R., D. Little, and R. Lytton, Fatigue and healing characterization of asphalt mixtures. Journal of Materials in Civil Engineering, 2003. 15(1): p. 75-83.

[3] Van Dijk, W., et al. The fatigue of bitumen and bituminous mixes. in Presented at the Third International Conference on the Structural Design of Asphalt Pavements, Grosvenor House, Park Lane, London, England, Sept. 11-15, 1972. 1972.

[4] Hopman, P.C., Kunst P.A.J.C and Pronk A.C., "A Renewed Interpretation Method for Fatigue Measurement, Verification of Miner's Rule," 4th Eurobitume Symposium, Volume 1, Madrid, 4-6 October 1989, pp 557-

561.

[5] Di Benedetto, H., Ashayer Soltani, A., and Chaverot, P.. “Fatigue damage for bituminous mixture: A pertinent approach.” J. Assoc. Asphalt Paving Technologists (AAPT), 1996, 6

[6] Lee, H. J.. “Uniaxial constitutive modeling of asphalt concrete using viscoelasticity and continuum damage theory.” PhD thesis, North Carolina State University, 1996, Raleigh, N.C.

[7] Rowe G M, Bouldin M G. Improved techniques to evaluate the fatigue resistance of asphaltic mixtures[C]//2nd Eurasphalt & Eurobitume Congress Barcelona, 2000.

[8] Rowe G M. Performance of asphalt mixtures in the trapezoidal fatigue test [J]. Asphalt Paving Technology, 1993, 62: 344-344.

[9] Kim Y R, Little D N, Lytton R L, et al. Use of dynamic mechanical analysis (DMA) to evaluate the fatigue and healing potential of asphalt binders in sand asphalt mixtures[J]. Asphalt Paving Technology: Association of Asphalt Paving Technologists-Proceedings of the Technical Sessions, 2002, 71:176-206.

[10] Van Dijk, W. and Visser, W., “The Energy Approach to Fatigue for Pavement Design,” Proceedings of Annual Meeting of the Association of Asphalt Paving Technologists (AAPT), 1977, Vol. 46, pp. 1–40.

[11] Ghuzlan, K.A. and S.H. Carpenter, Energy-derived, damage-based failure criterion for fatigue testing. Transportation research record, 2000. 1723(1): p. 141-149.

[12] Lytton R L. Characterizing asphalt pavements for performance[J]. Transportation Research Record, 2000, 1723(1): 5-16.

[13] Carpenter S H, Jansen M. Fatigue Behavior Under New Aircraft Loading Conditions. 353 In Aircraft/Pavement Technology: In the Midst of Change, seattle, Washington, 17-21 August 354 1997[J]. Edited by FV Hermann. American Socity of Civil Engineers, New York, 259-271.

[14] Bhasin A, Castelo Branco V T, Masad E, et al. Quantitative comparison of energy methods to characterize fatigue in asphalt materials[J]. Journal of materials in civil engineering, 2009, 21(2): 83-92.

[15] Pronk, A. C. and Hopman, P. C., “Energy Dissipation: The Leading Factor of Fatigue. Highway Research: Sharing the Benefits,” Proc., Conference of the United States Strategic Highway Research Progam, London, England, Telford, London, October 1990, pp. 225–267.

[16] Pronk A C. Evaluation of the dissipated energy concept for the interpretation of fatigue measurements in the crack initiation phase[J]. 1995.

[17] Shen, S. and S.H. Carpenter, Dissipated energy concepts for HMA performance: fatigue and healing. Vol. 67.

2006: Citeseer.

[18] British Standards Institution (2016), Bituminous mixtures – Material specifications. Asphalt Concrete, BS EN 13108-1:2016, London.

[19] British Standards Institution (2016), Bituminous mixtures – Test methods for hot mix asphalt – Part 35: Laboratory mixing, BS EN 12697-35: 2016, London.

[20] British Standards Institution (2019), Bituminous mixtures – Test methods for hot mix asphalt – Part 33: Specimen prepared by roller compactor, BS EN 12697-33: 2019, London.

[21] British Standards Institution (2007), Bitumen and bitumen binders, Measurement of density and specific gravity. Capillary-stoppered pyknometer method BS 2000-549:2007, London.

[22] British Standards Institution (2015), Methods of test for petroleum and its products, Bitumen and bituminous binders - Determination of needle penetration, BS EN 1426: 2015, London.

[23] British Standards Institution (2015), Methods of test for petroleum and its products, Bitumen and bituminous binders - Determination of the softening point. Ring and Ball method, BS EN 1427: 2015, London.

[24] British Standards Institution (2018), Bitumen and bituminous binders - Determination of dynamic viscosity of bituminous binder using a rotating spindle apparatus, BS EN 13302:2018, London.

[25] British Standards Institution (2017), Bituminous mixtures – Test methods for hot mix asphalt – Part 52: Conditioning to address oxidative ageing, CEN/TS 12697-52:2017, London.

[26] British Standards Institution (2018), Bituminous mixtures – Test methods for hot mix asphalt – Part 24: Resistance to fatigue, BS EN 12697-24: 2018, London.

[27] British Standards Institution (2017), Bituminous mixtures – Test methods for hot mix asphalt – Part 23: Determination of the indirect tensile strength of bituminous specimens, BS EN 12697-23:2017, London.

[28] Shen, Shihui, Xin. Energy Based Laboratory Fatigue Failure Criteria for Asphalt Materials[J]. Journal of Testing and Evaluation, 2011, 39(3).

[29] Menard, S., Applied logistic regression analysis (Vol. 106). Sage, 2002.

[30] Liu M, Udhe-Stone C, Goudar C T. Progress curve analysis of qRT-PCR reactions using the logistic growth equation.[J]. Biotechnology Progress, 2011, 27(5):1407-1414.

[31] Pastor-Barriuso R, Guallar E, Coresh J. Transition models for change-point estimation in logistic regression[J]. Statistics in Medicine, 2003, 22(7):1141.

[32] Rowe, G.M., Application of the dissipated energy concept to fatigue cracking in asphalt pavements. 1996, University of Nottingham.